

Room-temperature structural phase transition in the quasi-2D spin- $1/2$ Heisenberg antiferromagnet $\text{Cu}(\text{pz})_2(\text{ClO}_4)_2$

N. Barbero,^{1,*} M. Medarde,² T. Shang,² D. Sheptyakov,³ C. P. Landee,⁴ J. Mesot,^{1,5} H.-R. Ott,^{1,5} and T. Shiroka^{1,5,†}

¹Laboratorium für Festkörperphysik, ETH Zürich, CH-8093 Zurich, Switzerland

²Laboratory for Multiscale Materials Experiments, Paul Scherrer Institut, CH-5232 Villigen PSI, Switzerland

³Laboratory for Neutron Scattering and Imaging, Paul Scherrer Institut, CH-5232 Villigen PSI, Switzerland

⁴Department of Physics, Clark University, Worcester, Massachusetts 01610, USA

⁵Paul Scherrer Institut, CH-5232 Villigen PSI, Switzerland

$\text{Cu}(\text{pz})_2(\text{ClO}_4)_2$ (with *pz* denoting pyrazine $\text{C}_4\text{H}_4\text{N}_2$) is a two-dimensional spin- $1/2$ square-lattice antiferromagnet with $T_N = 4.24$ K. Due to a persisting focus on the low-temperature magnetic properties, its room-temperature structural and physical properties caught no attention up to now. Here we report a study of the structural features of $\text{Cu}(\text{pz})_2(\text{ClO}_4)_2$ in the paramagnetic phase, up to 330 K. By employing magnetization, specific heat, ^{35}Cl nuclear magnetic resonance, and neutron diffraction measurements, we provide evidence of a second-order phase transition at $T^* = 294$ K, not reported before. The absence of a magnetic ordering across T^* in the magnetization data, yet the presence of a sizable anomaly in the specific heat, suggest a structural order-to-disorder type transition. NMR and neutron-diffraction data corroborate our conjecture, by revealing subtle angular distortions of the pyrazine rings and of ClO_4^- counteranion tetrahedra, shown to adopt a configuration of higher symmetry above the transition temperature.

I. INTRODUCTION

As a notable physical realization of a quasi-2D Heisenberg antiferromagnet, $\text{Cu}(\text{pz})_2(\text{ClO}_4)_2$ has been a test case for investigating the competition between long-range magnetic order and quantum fluctuations [1, 2]. Its structure consists of stacks along the *c*-axis of well-isolated nearly-square layers of Cu^{2+} ions in the *ab*-plane, rotated by 45° with respect to the in-plane primitive vectors, as shown schematically in Fig. 1. Along the *c*-axis, each layer is shifted by half a unit cell along the *a*- and *b*-axes. Each Cu^{2+} ion is bridged to its four nearest-neighbors (NN) by $\text{C}_4\text{H}_4\text{N}_2$ pyrazine ligands, which provide the intralayer superexchange interaction. Two ClO_4^- perchlorate counteranions, linked to Cu^{2+} ions via one of the oxygen atoms in the O_4 tetrahedra, provide a sufficient interlayer separation along the *c*-axis, hence implying a negligible interlayer interaction. Overall, this results in a Cu^{2+} -ion arrangement of nearly-tetragonal symmetry [3]. The 3D antiferromagnetism (AFM) of $\text{Cu}(\text{pz})_2(\text{ClO}_4)_2$ has been extensively studied by inelastic neutron scattering (INS) [4], muon-spin rotation (μSR) [5], and nuclear magnetic resonance (NMR) [6] measurements. It has also been shown that applied magnetic fields along the *c*-axis strengthen the AFM order by suppressing the quantum fluctuations, hence enhancing T_N above its zero-field value of 4.24 K [4]. On the other hand, external hydrostatic pressure reduces T_N [6], most likely by enforcing 1D-type interactions [7], as suggested by results of density-functional theory (DFT) calculations on similar compounds [8, 9].

The crystal structure of $\text{Cu}(\text{pz})_2(\text{ClO}_4)_2$ was determined at 163 and 293 K from single-crystal x-ray diffraction data [10], obtaining a better refinement with the $C2/c$ space group in the first case and with the $C2/m$ space group in the latter. It was also observed that the four pyrazine moieties form two sets at low temperature, each of them characterized by a different tilting angle with respect to the *ab*-plane. The values of these angles are distinct at 163 K, but they become identical (65.8°) at 293 K. Along with x-ray diffraction patterns, Choi et al. [2] reported also infrared-spectroscopy data, used to track the evolution of the vibrational modes as a function of temperature. Upon heating, the latter measurements indicated a softening of the vibrational modes starting at approximately 180 K, related to the out-of-plane deformations of the pyrazine rings.

In this work, by combining data from NMR, specific-heat and neutron-diffraction experiments, we provide clear evidence for a *structural phase transition* occurring at $T^* = 294(1)$ K, not reported before in the literature. Our results indicate that the two initially different Cl sites become equivalent above T^* and that the symmetry of the individual pyrazine rings increases upon heating above T^* .

After introducing the experimental details in Sec. II, in Sec. III A and III B, we describe the material characterization via magnetization and specific-heat measurements. From these data, we identify the onset of the AFM order at T_N and of the structural transition at T^* , respectively. The ^{35}Cl NMR results discussed in Sec. III C clearly show the merging of the two lines upon heating, reflecting an increase in structure symmetry and allowing for an evaluation of the isotropic hyperfine coupling. Finally, to precisely identify the variations in bond lengths and angles, we employed neutron powder diffraction measurements, whose results are reported in Sec. III D. The combined data of our investigations indicate that the second-order structural phase transition is accompanied by subtle transformations in both the ClO_4^- tetrahedra and in the $\text{C}_4\text{H}_4\text{N}_2$ pyrazine ligands.

II. EXPERIMENTAL DETAILS

The $\text{Cu}(\text{ClO}_4)_2$ crystals were synthesized by dissolving $\text{Cu}(\text{ClO}_4)_2 \cdot 6\text{H}_2\text{O}$ and pyrazine in water with a drop of dilute $\text{HClO}_4(\text{aq})$, in order to prevent the precipitation of $\text{Cu}(\text{OH})_2$ and of CuCO_3 . The solution was then partially covered and left to evaporate slowly, with the crystals growing over several weeks. Finally, the mixture was filtered, the recovered crystals were washed in deionized water at $\sim 10^\circ\text{C}$, and dried in air. Since the samples are hygroscopic, they were stored in an inert-gas atmosphere [10]. Single crystals with a typical mass of ~ 80 mg were aligned with the *c*-axis (*hard* axis) parallel to the applied magnetic field, for both the magnetization- and NMR experiments. Given the easily identifiable *ab*-planes, delimited by smooth surfaces, the visual crystal alignment was achieved with an uncertainty of about 5° . For the neutron diffraction measurements, we used deuterated powder synthesized by following the same protocol, but employing deuterated reagents. The magne-

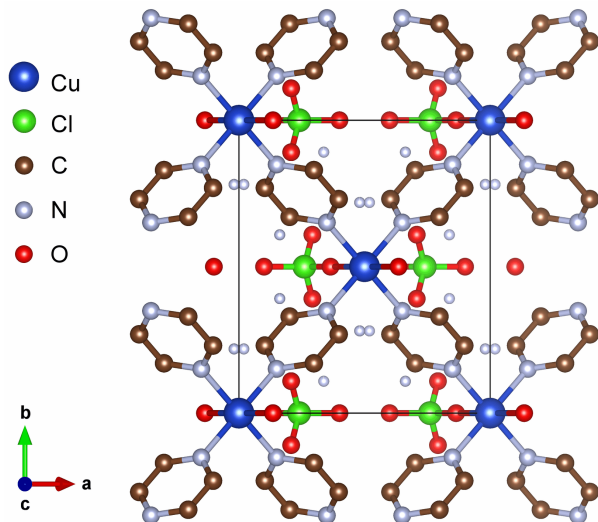


FIG. 1. A layer of $\text{Cu}(\text{pz})_2(\text{ClO}_4)_2$, whose $C2/m$ structure (space group no. 12) was determined from neutron diffraction data at 294 K. Each $\text{Cu}(\text{II})$ atom (blue) is linked via pyrazine rings (C = brown, N = gray) to four other copper ions, all lying in the ab -plane. The layers are spaced by perchlorate counteranions (Cl = green, O = red), lying along the interlayer c -axis direction. As described in the text and in Table I (see Appendix), the N and C atoms in the pyrazine rings and the O atoms in the perchlorate counteranions have different Wyckoff positions. Each counteranion contains a Cl site at the center and four O atoms at its vertices.

tization measurements were performed with a commercial magnetic property measurement system (MPMS) XL setup from 2 to 310 K in an applied magnetic field of 5 mT. The heat-capacity data were collected by means of a Quantum Design physical property measurement system (PPMS-9 T) by using the relaxation method, both upon heating and upon cooling, in a temperature range between 250 and 330 K.

The ^{35}Cl -NMR study comprised lineshape and spin-lattice relaxation time measurements in a 7.063-T field, corresponding to a Larmor frequency of 29.4664 MHz for the spin-3/2 ^{35}Cl quadrupolar nuclei. NMR signals were detected by employing a standard spin-echo sequence, consisting in $\pi/2$ and π pulses of 2 and 4 μs , respectively, with recycle delays ranging from 0.6 to 0.2 s for temperatures in the 4–310 K range. The NMR lineshapes were obtained from fast Fourier transforms (FFT) of the echo signals. The spin-lattice relaxation times T_1 were measured via the inversion-recovery method using a π - $\pi/2$ - π pulse sequence.

Neutron diffraction experiments were performed at the HRPT diffractometer (high-resolution powder diffractometer for thermal neutrons) at the SINQ facility of the Paul Scherrer Institute (PSI) in Villigen, Switzerland. Several patterns were recorded between 260 and 330 K, using two different wavelengths ($\lambda = 1.494 \text{ \AA}$ and 1.886 \AA) of the high-intensity mode (2 θ primary-beam collimation) [11]. The sample was placed in an 8-mm-diameter vanadium cylinder under helium atmosphere and sealed with indium wire. The cylinder was then introduced into a cryofurnace whose contribution to the neutron-count background was minimized by means of an oscillating radial collimator. All the patterns were refined by using the Rietveld refinement FullProf suite [12].

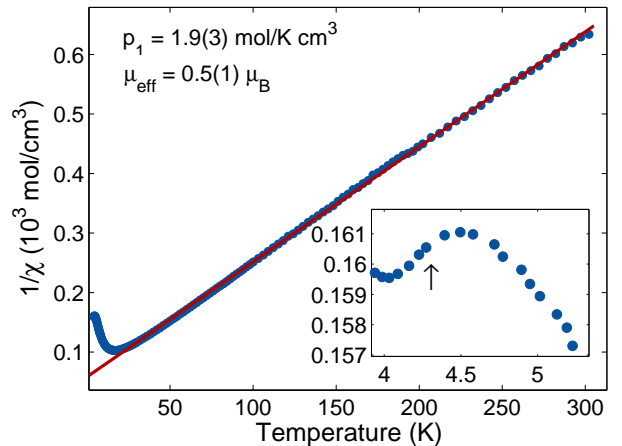


FIG. 2. $1/\chi(T)$, as measured at 5 mT. The linear fit (red line) to the data in the paramagnetic regime ($T > 20$ K) implies an effective magnetic moment of $0.5(1) \mu_B$, while the negative intercept on the T axis indicates AFM interactions among the Cu^{2+} ions. Inset: low-temperature $1/\chi(T)$ data. The arrow at $T_N = 4.24$ K indicates the inflection point, considered as the onset of AFM order [6].

III. RESULTS AND DISCUSSION

A. Magnetization measurements

The inverse magnetic susceptibility $1/\chi(T)$ measured at 5 mT (see Fig. 2) indicates an effective magnetic moment, $\mu_{\text{eff}} = 0.5(1) \mu_B$. Its value, far smaller than the corresponding Cu single-ion spin-only magnetic moment ($1.73 \mu_B$), suggests the presence of strong quantum fluctuations. As previously reported [4], an enhancement of μ_{eff} in higher magnetic fields may be interpreted as a field-induced suppression of the quantum fluctuations. Besides the clear anomaly at $T_N \sim 4.2$ K, the $\chi_m(T)$ response remains paramagnetic up to 300 K, thus excluding the magnetic nature of the transition observed at $T^* = 294$ K (see below).

B. Specific-heat measurements

The heat capacity data vs. temperature, collected between 250 and 330 K upon both heating and cooling, are shown in Fig. 3. The significant and overlapping (i.e., hysteresis-free) anomalies both peak at 293 K and indicate the existence of a previously unnoticed second-order phase transition in this temperature range. The independence of the transition from the applied magnetic field (of 5 T in this case, see inset in Fig. 3) and the absence of an anomaly in the magnetic susceptibility (see Fig. 2), rule out a magnetic origin of the transition and suggest the transition at T^* to be of *structural character*. From the heat-capacity data, we calculated numerically the entropy $\Delta S(T) = \int_{T_0}^T C_p d(\ln T)$, with T_0 being a reference temperature. Since across T^* we find $\Delta S(T) \sim R$ ($= 8.31 \text{ JK}^{-1} \text{ mol}^{-1}$), this suggest an order-to-disorder (i.e., a non displacive) type of structural transition (see below).

C. Nuclear magnetic resonance measurements

The ^{35}Cl NMR lines measured at different temperatures are shown in Fig. 4. The formation of two magnetic sublat-

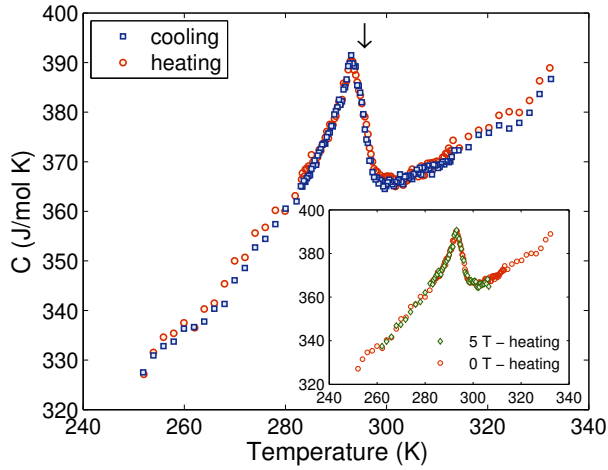


FIG. 3. The temperature dependence of the heat capacity measured upon heating and cooling showing the lack of hysteresis. The arrow indicates $T^* = 294$ K. Inset: the coinciding 0- and 5-T datasets rule out heat-capacity changes in the applied magnetic field range.

tices in the AFM phase, below 4.24 K [6], is clearly manifested in the line splitting and broadening of the $T = 4$ K dataset. Most important to us is the line behavior in the high-temperature regime. Figure 5 shows the evolution of the peak positions (a) and of their separation (b) with temperature. Below $T^* = 294$ K, the two distinct NMR lines correspond to two crystallographically inequivalent chlorine sites. Their merging at T^* suggests a structural transition of certain structural sub-units to a higher symmetry, which reestablishes the site equivalence and preserves it upon heating up to at least 330 K. This transition is even better illustrated by the peak-to-peak distance vs. temperature plot [see Fig. 5(b)]. The peak separation exhibits first a shallow maximum centered at 175 K, then it continuously decreases, to finally vanish at $T^* = 294$ K, a value very close to that of the maximum in the heat-capacity $C(T)$ data (293 K).

Note that both the Knight shift and the static susceptibility [6] (i.e., the magnetization data), exhibit a very similar temperature dependence. In particular, the susceptibility data were compared to those calculated by quantum Monte Carlo simulations and, upon assuming the validity of a 2D Heisenberg model on a square lattice (see Fig. 3 in Ref. [6]), an excellent agreement was found.

By relating the frequency shifts $K_s(T)$ of the two ^{35}Cl NMR lines to the susceptibility data $\chi(T)$ at the corresponding temperatures, we obtain the so-called Clogston-Jaccarino plot [13], with T as an implicit parameter. This is shown in Fig. 6 and was used to evaluate the amplitude of the hyperfine interaction A_{hf} . In our case, this is the same for both ^{35}Cl sites, $A_{\text{hf}} = -10(5) \text{ mT}/\mu_B$ (see parallel fit lines in Fig. 6), and was calculated by means of [14]

$$K_s = gA_{\text{hf}}\chi + K_{\text{orb}}, \quad (1)$$

by assuming a standard electronic g factor of 2.0. By extrapolating the straight line fits to $\chi_m = 0$ (see Fig. 6), we obtain an orbital (i.e., temperature independent) shift K_{orb} of 0.13% for the upper line and of 0.03% for the lower one. Above T^* , the shift of the single NMR line extrapolates to 0.108%, in excellent agreement with the typical values of ^{35}Cl chemical shift in the perchlorates (e.g., 0.105% in KClO_4) [15]. While the latter reflects the undistorted geometry of the ClO_4^- tetrahedra, the rather different K_{orb} values

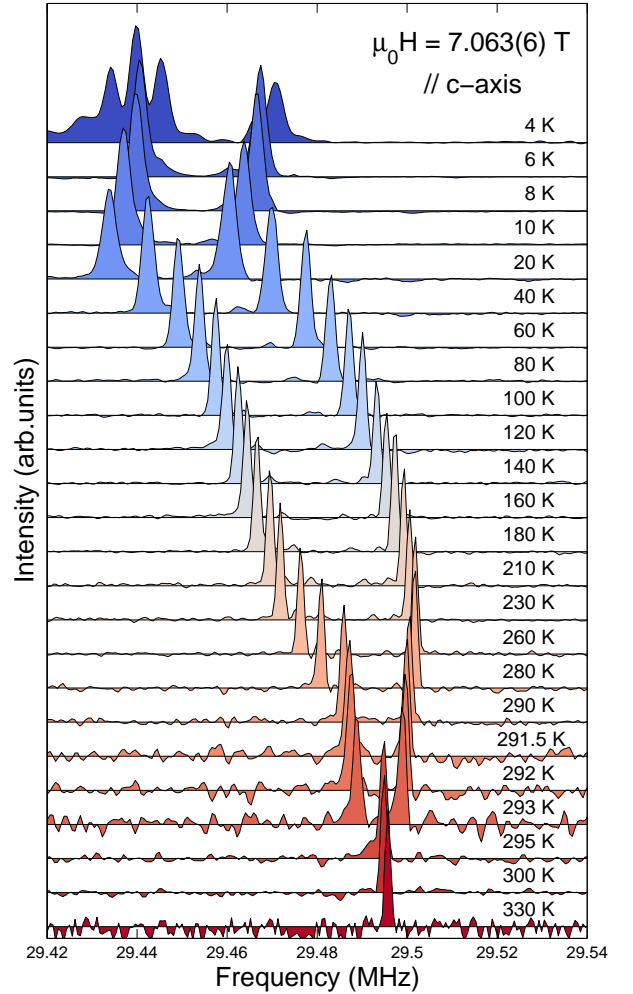


FIG. 4. Evolution of the ^{35}Cl NMR line shape and position with temperature. Note that at room temperature $\text{Cu}(\text{pz})_2(\text{ClO}_4)_2$ exhibits a positive paramagnetic shift of $\sim 0.1\%$, with respect to the Larmor frequency (29.466 MHz in a 7.063-T magnetic field). At $T^* = 294$ K, the two NMR lines resulting from the two inequivalent chlorine sites merge into a single peak, indicating that the structural transformation of the ClO_4^- tetrahedra is complete.

observed below T^* , differing by approximately +25% and -75% , respectively, are strong indicators of a significant deviation from the structural configuration adopted above T^* . Considering that the ^{35}Cl nuclei are located inside the tetrahedra, the change of K_{orb} across T^* has to be related to a static or dynamic modification of the tetrahedra, as confirmed by neutron diffraction experiments (see below).

Since the NMR spin-lattice relaxation rates $1/T_1$ are known to be very sensitive to phase transitions [16], [17] we performed detailed T_1 measurements in the temperature range between 280 and 320 K. The relaxation-rate data collected by means of the inversion-recovery method (see Fig. 7), confirm the presence of an anomaly at 295(1) K, compatible with the T^* value, here defined as the merging point of the two distinct ^{35}Cl NMR lines. The T_1 values were determined from fits using the formula relevant for spin-3/2 nuclei [18]:

$$M_z(t) = M_0[1 - f \cdot (0.9 \cdot e^{-(6t/T_1)^\lambda} + 0.1 \cdot e^{-(t/T_1)^\lambda})]. \quad (2)$$

Here M_0 is the saturation value of nuclear magnetization, the parameter f is ideally 2 for a full inversion, while λ (≤ 1) is a stretching coefficient which accounts for a possible

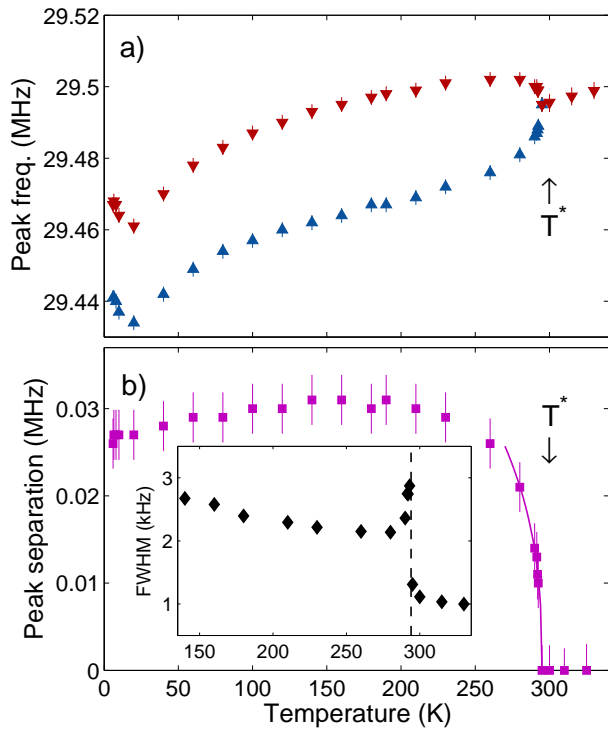


FIG. 5. ^{35}Cl NMR peak positions vs. temperature (a). Despite a general increase in frequency with temperature, the peak separation (b) stays mostly constant (ca. ~ 30 kHz), to smoothly go to zero at $T^* = 294$ K (see arrows). The line is a fit to $(1 - T/T^*)^\beta$, with $\beta = 0.45(5)$. Inset: upon heating, the NMR linewidth shows a clear drop at T^* (dashed line) indicative of a transition to a configuration with higher local symmetry.

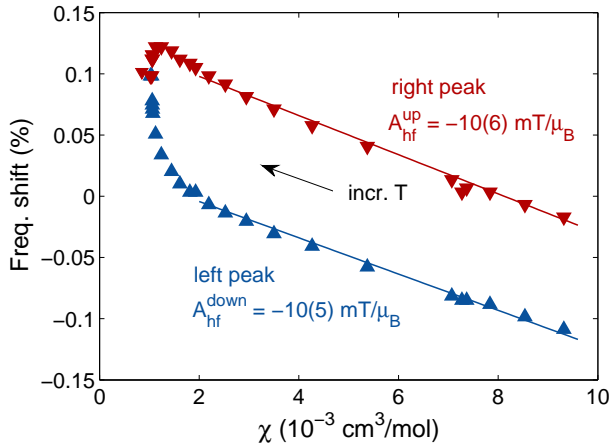


FIG. 6. The Clogston-Jaccarino $K_s(T)$ vs. $\chi(T)$ plot for the two inequivalent chlorine sites. The almost identical slopes result in the same hyperfine coupling value, $A_{\text{hf}} = -10(5) \text{ mT}/\mu_B$. The purely linear behavior is modified when the NMR signals start to merge. The arrow indicates the direction of the increasing temperature.

distribution of spin-lattice relaxation times around the mean T_1 value. In our case, we find $f \sim 1.6(2)$ and $\lambda \sim 0.82(9)$ in the entire investigated temperature range. Both parameters exhibit a smooth variation across T^* , once more suggesting the structural character of the transition. Since the two ^{35}Cl NMR lines show very similar T_1 values, in the following we refer to only one of them, i.e., to the low-frequency signal.

The two datasets shown in Fig. 7 correspond to the relaxation rates $1/T_1$ measured upon cooling (blue) and heat-

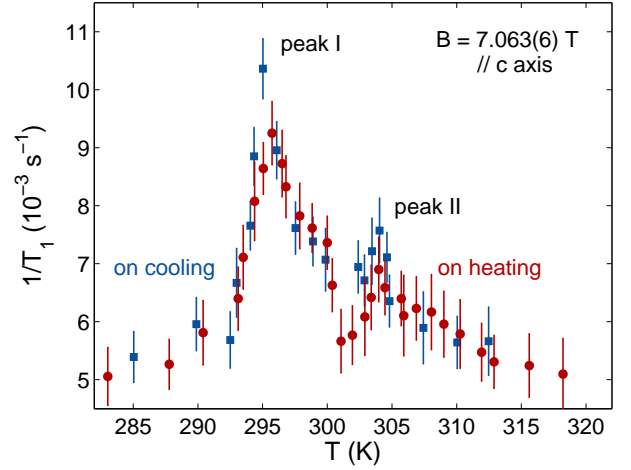


FIG. 7. ^{35}Cl NMR spin-lattice relaxation rate $1/T_1$ vs. temperature measured upon heating (red circles) and cooling (blue squares). Both datasets exhibit a main peak (I) at 295 K and a smaller secondary peak (II) at 304 K. To compensate for a known calibration offset, data measured upon heating were shifted by -2.0 K.

ing (red). In both cases a clear peak is observed at 295 K, with a small yet distinct anomaly peaking at $T^{**} = 304$ K. The latter most likely reflects a minor change in the local atomic configuration, as suggested by neutron-diffraction data (see below). The lack of hysteresis, confirmed also by the previously mentioned heat-capacity data, is indicative of a second-order phase transition. In the covered temperature range (up to 320 K), no other peaks or anomalies were detected. Earlier NMR studies of pure pyrazine [19, 20] reported two anomalies at similar temperatures (301.5 K and 309 K, respectively), which were interpreted as partial order-to-disorder transitions.

This similarity poses the question of whether this structural transition is also a feature of other molecular-copper complexes containing stacked pyrazine rings, such as the one-dimensional chains in $\text{Cu}(\text{pz})(\text{NO}_3)_2$ [21] or the two-dimensional $\text{Cu}(\text{pz})_2\text{X}_2$ family [2] (here X indicates a counterion, e.g., ClO_4^- , BF_4^- , and PF_6^-). The role of counterions and ligands in $\text{Cu}(\text{pz})_2(\text{ClO}_4)_2$ was previously investigated by DFT calculations [8]. These indicate that relevant structural changes with static or dynamic character may occur in $\text{Cu}(\text{pz})_2(\text{ClO}_4)_2$, and consist of shearing-like distortions of the pyrazine rings [8], in hydrogen-bonding effects [22], or in the re-orientation, deformation, and freezing of the perchlorate counteranions [8]. The latter work reported a positive correlation between the intensity of AFM exchange interactions and the shearing-like distortions of pyrazine rings, suggesting that this may also be observed in other $\text{Cu}(\text{pz})$ -based magnets. Furthermore, if the presence of counterions is neglected, even tiny differences in the interatomic distances in the $\text{Cu}-\text{N}\cdots\text{N}-\text{Cu}$ magnetic pathways give rise to sizable differences in the intensity of in-plane exchange interactions, regardless of the canting angle of the pyrazine ligands. Theoretical calculations considered also different types of counterions and concluded that the spin density on the central pyrazine and, hence, the magnetic exchange interaction, is enhanced by the more electronegative external atoms, as is the case of ClO_4^- . To assess whether, in our case, the detected phase transitions are due to one or more of the above mentioned changes predicted by DFT calculations, we had to perform neutron-diffraction experiments.

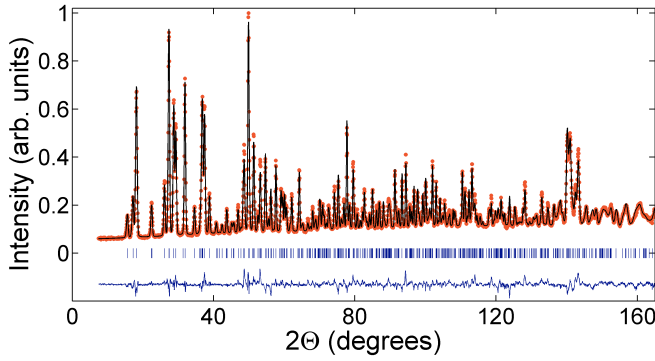


FIG. 8. A typical neutron-diffraction pattern measured at 294 K using $\lambda = 1.8857 \text{ \AA}$. The orange circles correspond to the observed pattern and the black solid line to the Rietveld fit obtained using the $C2/m$ space group. The positions of the Bragg reflections and the difference between the observed and calculated patterns are shown in blue.

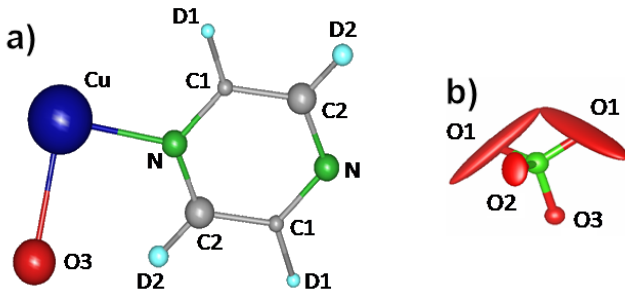


FIG. 9. (a) Structural fragment of the pyrazine ring with labels identifying each atom. (b) Thermal ellipsoids of oxygen atoms in the ClO_4^- perchlorate anions at 294 K. Note the large displacements of the two O1 atoms.

D. Neutron diffraction

The magnetization, specific-heat, and NMR results shown in the previous sections suggest a structural origin for the two transitions at $T^* = 294 \text{ K}$ and $T^{**} = 304 \text{ K}$. To closely monitor the evolution of the crystal structure between 260 and 330 K we performed systematic neutron powder-diffraction measurements. The initial structure refinement at 295 K, i.e., just above the transition, was carried out by assuming as valid the $C2/m$ space group, previously proposed in the literature for the structure at 293 K [1]. A representative Rietveld fit is shown in Fig. 8.

The systematic extinctions when using this space group were found compatible with the high-resolution synchrotron x-ray powder diffraction data collected above and below the transition (260 and 295 K), and refined by using the Le Bail method [23]. Besides $C2/m$, we also tried its subgroups $C2$ and Cm , indistinguishable in terms of solely systematic extinctions, but providing additional degrees of freedom, see Table I. The three groups were also tested with neutron data recorded at 260 and 295 K. Rietveld refinements using the $C2$ group, for which the absence of a mirror plane implies $4/4/2$ different C/D/N Wyckoff positions (instead of $2/2/1$ in the $C2/m$ case), provided slightly more realistic results for the environment of Cl in the perchlorate groups and better reliability indexes. However, the larger number of free parameters resulted in the appearance of correlations and less stable fits. $C2/m$, which imposes additional restrictions, resulted in an improved fit stability and less

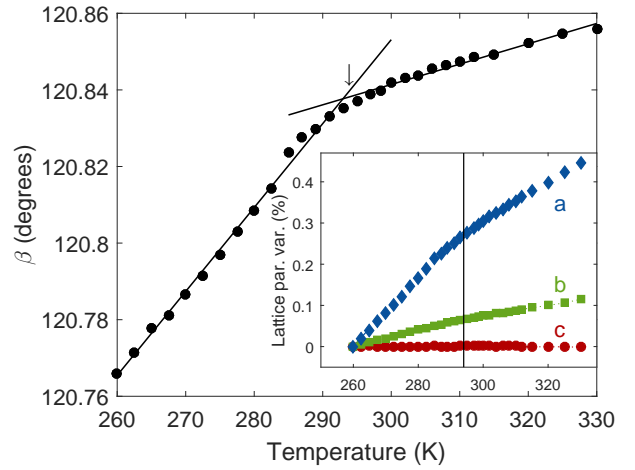


FIG. 10. Relative variation of the lattice parameters a , b , and c (inset) and of the monoclinic angle β (main panel) with temperature. The interlayer axis (c) is almost constant, the b axis increases smoothly, whereas the a axis exhibits a tiny kink close to T^* (vertical line). The monoclinic angle $\beta(T)$, too, shows a clear change of slope across the transition (arrow).

correlations. Hence $C2/m$ was finally preferred for the description of the crystal structure across the full 260–330 K temperature range. The obtained values of the atomic coordinates and Debye-Waller factors (see Figs. 9 and 12), and in particular those of two of the oxygens in the perchlorate groups, should be considered with caution as they represent averages of the atomic positions in the actual (disordered) crystal structure. The resulting structural parameters and the agreement factors obtained at 295 K with the two space groups are reported in Table I (see Appendix).

Figure 10 shows the temperature evolution of the four lattice parameters (a , b , c , and the monoclinic angle β), as obtained from fits based on the $C2/m$ space group. While β exhibits a clear change in slope close to T^* , no evident features at the transition temperature were observed in the remaining lattice parameters, except for a tiny change in slope of $a(T)$ close to T^* . From the NMR data, modifications related to the static (or dynamic) configuration of the perchlorate tetrahedra are expected. The above anomalies in the lattice parameters may also reflect the atomic rearrangements within the unit cell.

In spite of the above mentioned restrictions, the structural parameters obtained from fits based on the $C2/m$ space group provide information not only on the atomic rearrangements, but also on the average structural disorder through the analysis of the Debye-Waller factors. The latter quantify the mean-square displacements U_{ij} (ADP, i.e., atomic displacement parameter) of each atom from its average position. In harmonic crystals, U_{ij} -s can be interpreted in terms of time-averaged mean-square displacements resulting from the normal modes of vibration. In disordered materials, however, they can also capture displacements due to positional disorder [24–26] [27]. The β_{ij} values, defined as $\beta_{ij} = 8\pi^2 U_{ij} x_i^* x_j^* / 4$, with x_i^* and x_j^* the reciprocal-cell parameters, were obtained from Rietveld fits with the FullProf suite package [12].

As shown in Fig. 9(b), the thermal ellipsoids described by the ADPs are remarkably large for two of the three oxygen atoms that are not bound to a Cu magnetic site [here bound to O3 – see Fig. 9(a)]. The two oxygen atoms labeled O1

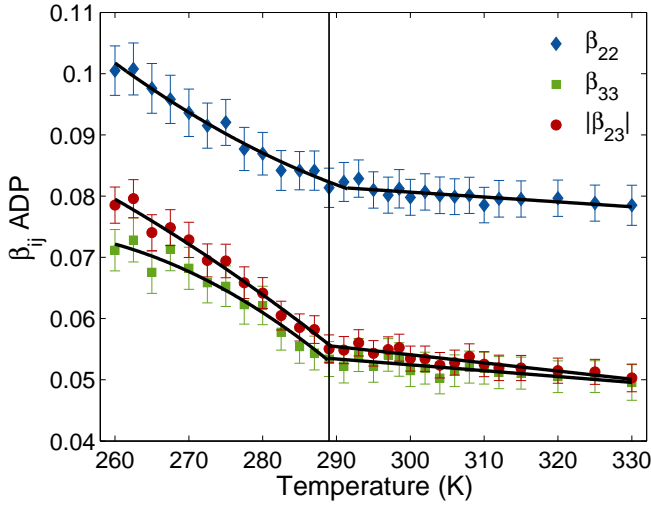


FIG. 11. Temperature dependence of the diagonal β_{22} (blue diamonds) and β_{33} (green squares) O1 ADPs and of the absolute value of the off-diagonal β_{23} term (red circles). The crossing of the parabolic- and linear fits (black solid lines) was used to better define the position of the anomaly at ~ 290 K (vertical line).

exhibit the largest displacements, and their β_{22} , β_{33} , and β_{23} ADPs show clear anomalies across T^* (see Fig. 11). From 260 K to 290 K the diagonal terms β_{22} and β_{33} clearly decrease, to become almost constant above T^* . The same reduction (in absolute value) is observed in the negative off-diagonal term β_{23} , which also saturates above 290 K. Such general reductions of the absolute ADP values indicate a decrease of disorder above T^* . The decrease of local disorder within the tetrahedra upon heating seems at first counterintuitive. Yet, it is in line with NMR results, which also indicate the number of inequivalent Cl sites (inside the ClO_4^- tetrahedra) to decrease upon heating from two to one at T^* . A possible explanation for the enhanced degree of disorder at lower temperatures might be given by the coexistence of two competing oxygen positions. Note that significantly large ADP values persist also above T^* , most likely indicating the presence of a residual positional disorder.

As shown in Fig. 12, the transition at T^* also involves subtle structural anomalies related to a distortion and re-orientation of the four pyrazine rings. For instance, the N–D1 distance first increases up to 288 K and then saturates, whereas the y and z atomic coordinates of the N atoms first rapidly decrease down to T^* and then continue decreasing with a reduced rate or saturate, respectively. We recall that x , y , and z are the atomic coordinates, referred to the basis vectors a , b , and c , respectively. As for the x coordinate, it increases linearly across the covered temperature range, without showing any evident anomalies. Incidentally, the crossing of the x - and y coordinate values at about 308 K suggests a more regular in-plane arrangement of the pyrazine ligands above the second, yet much weaker, transition at T^{**} . This corresponds to the pyrazine rings becoming closer to regular undeformed hexagons. We note also that such rings are not perfectly flat. Nevertheless, considering the small deviations from an ideal plane, we still can define a dihedral angle θ_d between the average plane of the pyrazine rings and the basal plane of Cu octahedra. The temperature dependence of the dihedral angle is shown in Fig. 12(a) (right scale). This angle, very close to the values reported in the literature [10], decreases with temperature. Albeit

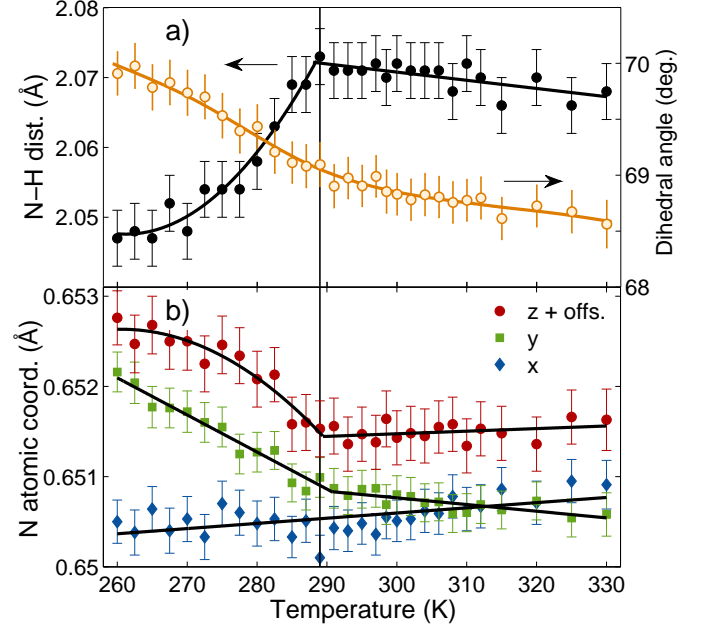


FIG. 12. Temperature-dependence of the N–D1 distance (a) and of the atomic coordinates of the N atoms (b). In all cases, the crossing of parabolic- (linear-) and linear fits (black solid lines) was used to define the position of the anomaly at ~ 290 K (vertical line). In (b), the x and y coordinates cross at about 308 K. For clarity, the z values were vertically offset by 0.647 Å. The dihedral angle, also shown in (a), decreases with temperature and exhibits an inflection point at ~ 290 K.

weakly, the structural transition at ~ 290 K is here reflected in an inflection point in $\theta_d(T)$.

In any case, such modifications are subtle and modest in magnitude. We also note that the small mismatch between the transition temperature T^* , established as outlined in Secs. III B and III C, and the anomalies in the neutron-diffraction data is most likely due to temperature control and calibration issues, difficult to control exactly in experiments at room temperature. Moreover, we recall that the Cu–N and Cu–O3 distances do not exhibit clear anomalies at T^* and that the ratio $d(\text{Cu–N})/d(\text{Cu–O3})$, reflecting the degree of the Jahn-Teller distortion of the octahedra centered at Cu sites, has a constant value of 1.14 ± 0.08 . Finally, both the in-plane N–Cu–N- and the apical O–Cu–N angles are close to 90° and tend to the exact value of 90° upon increasing temperature. The absence of significant changes in these angles, which control the overlap of the CuN and CuO orbitals, indicates that the phase transition reported here does not imply sizable changes in the strength of the superexchange interactions.

To provide a possible explanation for the above observations, we recall that structural phase transitions can be classified as either displacive or order-disorder, usually considered as mutually exclusive. The latter consists in the transition from a configuration where one or more sites exhibit split occupancies to a more ordered one within the same set of atomic positions. From our neutron-diffraction and $C_p(T)$ measurements, we conclude that the observed transition is a second-order structural transition of the order-disorder type (with some possible residual displacive effects). In fact, below T^* , two locally different Cl sites can be distinguished and, hence, the system is disordered. Above T^* , despite the

established equivalence of the two Cl sites, some residual disorder persists, most likely due to the co-existence of two similar configurations of the perchlorate subunits.

IV. CONCLUSION

By combining the results of magnetization-, specific-heat-, NMR-, and neutron-diffraction experiments, we identified a previously unnoticed second-order phase transition at $T^* = 294$ K in $\text{Cu}(\text{pz})_2(\text{ClO}_4)_2$ and determined its order-to-disorder structural character. ^{35}Cl NMR measurements indicate the presence of two inequivalent ^{35}Cl sites which persists, upon heating, up to the transition temperature. Interestingly, the distance in frequency between the two ^{35}Cl NMR lines starts reducing from 175 K, i.e., the temperature at which a softening of the vibrational modes related to the pyrazine rings was previously observed. Above T^* , the measured NMR orbital shift is compatible with typical values of the ^{35}Cl nucleus in a tetrahedral environment. Below T^* , instead, it assumes two significantly different values, with opposite signs for the two distinct sites, thus revealing strong deviations from the ideal tetrahedral geometry. The spin-lattice relaxation-rate data allowed us to precisely identify T^* and to observe also a minor anomaly at $T^{**} = 304$ K, attributable to secondary structural distortions. The refinement of the neutron-diffraction patterns, assuming the validity of the $C2/m$ space group, was used to monitor the temperature dependence of all the structural parameters. A detailed analysis indicates that the reported transition affects the perchlorate ClO_4^- tetrahedra, which adopt a more regular and ordered arrangement above T^* . The relatively high values of the atomic displacements indicate the persistence of some positional disorder also above

the transition, most likely due to the competition between two possible oxygen-site positions, almost degenerate in energy. Similarly, reorientations of the pyrazine rings, occurring at the transition, are reflected in anomalies in the N–H distance and in the nitrogen atomic coordinates. As shown by magnetization- and specific-heat data, these subtle structural modifications do not affect the magnetic properties of $\text{Cu}(\text{pz})_2(\text{ClO}_4)_2$ in the covered temperature range. Future DFT calculations, which account for positional disorder and geometric distortions, are expected to provide further insight into the significance of the structural phase transition reported here.

ACKNOWLEDGMENTS

This work is based on experiments performed at the Swiss spallation neutron source SINQ and the Swiss Light Source SLS, both at the Paul Scherrer Institute, Villigen, Switzerland. A special thank goes to N. Casati for supporting our preliminary x-ray experiments at the Materials Science Beamline (SLS). The authors thank M. Chinotti, D. Gawryluk, and M. Turnbull for helpful discussions and assistance. This work was financially supported in part by the Schweizerische Nationalfonds zur Förderung der Wissenschaftlichen Forschung (SNF), Grant no. 200021-169455.

APPENDIX

A. Structural refinement comparison between the $C2/m$ and $C2$ space groups at 294 K

$T = 295$ K	$C2/m$ model	$C2$ model
a (Å)	9.78047(9)	9.78070(7)
b (Å)	9.77594(9)	9.77589(7)
c (Å)	8.16470(9)	8.16488(7)
β (°)	120.8361(7)	120.8353(6)
Cu (2a)/(2a)	[0, 0, 0]	[0, 0, 0]
U_{iso} (Å ²)	0.0118(9)	0.0126(9)
Cl (4i)/(4c)	[0.2402(4), 0, 0.5391(5)]	[0.2599(4), 0.4925(16), 0.4607(5)]
U_{iso} (Å ²)	0.012(3)	0.0292(10)
O1 (8j)/(4c)	[0.2052(9), 0.1075(9), 0.6031(11)]	[0.3071(18), 0.588(3), 0.388(3)]
U_{11} (Å ²)	0.057(5)	0.031(7)
U_{22} (Å ²)	0.393(14)	0.48(5)
U_{33} (Å ²)	0.128(6)	0.100(13)
U_{12} (Å ²)	0.061(6)	−0.051(14)
U_{13} (Å ²)	−0.030(4)	−0.035(7)
U_{23} (Å ²)	−0.195(7)	0.21(2)
U_{iso} (Å ²)	0.193(8)	0.20(2)
O1' (−)/(4c)	−	[0.2713(19), 0.374(3), 0.397(3)]
U_{11} (Å ²)	−	0.061(10)
U_{22} (Å ²)	−	0.217(16)
U_{33} (Å ²)	−	0.176(18)
U_{12} (Å ²)	−	0.006(10)
U_{13} (Å ²)	−	0.012(11)
U_{23} (Å ²)	−	−0.173(14)
U_{iso} (Å ²)	−	0.151(15)

O2 (4i)/(4c)	[0.4010(7), 0, 0.5868(9)]	[0.1025(6), 0.504(2), 0.4146(9)]
$U_{11}(\text{Å}^2)$	–	0.015(3)
$U_{22}(\text{Å}^2)$	–	0.069(5)
$U_{33}(\text{Å}^2)$	–	0.067(5)
$U_{12}(\text{Å}^2)$	–	0.005(6)
$U_{13}(\text{Å}^2)$	–	0.009(3)
$U_{23}(\text{Å}^2)$	–	0.003(7)
$U_{\text{iso}}(\text{Å}^2)$	0.042(4)	0.047(4)
O3 (4i)/(4c)	[0.1363(7), 0, 0.3366(8)]	[0.3643(6), 0.503(2), 0.6617(8)]
$U_{\text{iso}}(\text{Å}^2)$	0.0311(13)	0.0335(13)
C1 (8j)/(4c)	[0.8968(3), 0.7691(3), 0.1448(4)]	[0.8948(10) 0.2307(14) 0.1506(11)]
$U_{\text{iso}}(\text{Å}^2)$	0.0145(7)	0.0168(5)*
C2 (8j)/(4c)	[0.7985(3), 0.6701(3), 0.1524(4)]	[0.2996(9) 0.8400(15) 0.1504(12)]
$U_{\text{iso}}(\text{Å}^2)$	0.0190(7)	0.0168(5)*
C3 (–)/(4c)	–	[0.0997(10), 0.7683(14), 0.8572(11)]
$U_{\text{iso}}(\text{Å}^2)$	–	0.0168(5)*
C4 (–)/(4c)	–	[0.7037(9), 0.1779(14), 0.8445(12)]
$U_{\text{iso}}(\text{Å}^2)$	–	0.0168(5)*
D1 (8j)/(4c)	[1.0197(5), 0.7807(4), 0.2700(6)]	[0.0283(9), 0.2351(14), 0.2558(9)]
O_{cc}	0.978(2)*	0.961(7)*
$U_{\text{iso}}(\text{Å}^2)$	0.0428(12)	0.0254(9)*
D2 (8j)/(4c)	[0.8379(5), 0.6088(4), 0.2768(5)]	[0.3453(8), 0.9067(14), 0.2672(9)]
O_{cc}	0.978(2)*	0.961(7)*
$U_{\text{iso}}(\text{Å}^2)$	0.0372(10)	0.0254(9)*
D3 (–)/(4c)	–	[0.9892(8), 0.7973(14), 0.7166(10)]
O_{cc}	–	0.961(7)*
$U_{\text{iso}}(\text{Å}^2)$	–	0.0254(9)*
D4 (–)/(4c)	–	[0.6732(8), 0.1254(14), 0.7153(10)]
O_{cc}	–	0.961(7)*
$U_{\text{iso}}(\text{Å}^2)$	–	0.0254(9)*
N1 (8j)/(4c)	[0.6505(2), 0.65082(20), 0.0041(3)]	[0.8503(6), 0.1551(15), 0.9987(8)]
$U_{\text{iso}}(\text{Å}^2)$	0.0096(4)	0.0141(5)*
N2 (–)/(4c)	–	[0.1512(6), 0.8534(15), 0.0060(8)]
$U_{\text{iso}}(\text{Å}^2)$	–	0.0141(5)*
λ (Å)	1.494 1.886	1.494 1.886
χ^2	5.18 8.54	3.27 5.06
R_{exp}	4.50 3.49	4.48 3.48
R_{wp}	10.2 10.2	8.10 7.82
R_p	9.37 9.14	7.53 7.25

Table I. Structural parameters as determined from neutron powder diffraction at $T = 295$ K, using the space groups $C2/m$ and $C2$, respectively [28]. For the last group, that is non-centrosymmetric, the origin is floating. For that reason the y -coordinate of Cu has been fixed to zero, matching the Cu position in $C2/m$. To further facilitate comparisons, the setting for the monoclinic cell was chosen to be the same as in reference [10]. For every space group the fits were carried out using a single structural model to refine simultaneously the data recorded at $\lambda = 1.494$ and 1.886 Å. The related .cif file with the refinement parameters can be found in the Supplemental Material [29].

- * Corresponding author: nbarbero@phys.ethz.ch
- † Corresponding author: tshiroka@phys.ethz.ch
- [1] J. Darriet, M. S. Haddad, E. N. Duesler, and D. N. Hendrickson, Crystal structure and magnetic properties of bis(pyrazine)-copper(II) perchlorate, $\text{Cu}(\text{pyz})_2(\text{ClO}_4)_2$, a two-dimensional Heisenberg antiferromagnet, *Inorg. Chem.* **18**, 2679 (1979).
 - [2] J. Choi, J. D. Woodward, J. L. Musfeldt, C. P. Landee, and M. M. Turnbull, Vibrational properties of $\text{Cu}(\text{pz})_2(\text{ClO}_4)_2$: Evidence for enhanced low-temperature hydrogen bonding in square $S = 1/2$ molecular antiferromagnets, *Chem. Mater.* **15**, 2797 (2003).
 - [3] C. P. Landee and M. M. Turnbull, Recent developments in low-dimensional copper(II) molecular magnets, *Eur. J. Inorg. Chem.* **13**, 2266 (2013).
 - [4] N. Tsyruilin, F. Xiao, A. Schneidewind, P. Link, H. M. Rønnow, J. Gavilano, C. P. Landee, M. M. Turnbull, and M. Kenzelmann, Two-dimensional square-lattice $S = 1/2$ antiferromagnet $\text{Cu}(\text{pz})_2(\text{ClO}_4)_2$, *Phys. Rev. B* **81**, 134409 (2010).
 - [5] T. Lancaster, S. J. Blundell, M. L. Brooks, P. J. Baker, F. L. Pratt, J. L. Manson, M. M. Conner, F. Xiao, C. P. Landee, F. A. Chaves, S. Soriano, M. A. Novak, T. P. Papageorgiou, A. D. Bianchi, T. Herrmannsdörfer, J. Wosnitza, and J. A. Schlueter, Magnetic order in the $S = 1/2$ two-dimensional molecular antiferromagnet copper pyrazine perchlorate $\text{Cu}(\text{pz})_2(\text{ClO}_4)_2$, *Phys. Rev. B* **75**, 094421 (2007).
 - [6] N. Barbero, T. Shiroka, C. P. Landee, M. Pikulski, H.-R. Ott, and J. Mesot, Pressure and magnetic field effects on a quasi-two-dimensional spin-1/2 Heisenberg antiferromagnet, *Phys. Rev. B* **93**, 054425 (2016).
 - [7] N. D. Mermin and H. Wagner, Absence of ferromagnetism or antiferromagnetism in one- or two-dimensional isotropic Heisenberg models, *Phys. Rev. Lett.* **17**, 1133 (1966).
 - [8] S. Vela, J. Jornet-Somoza, M. M. Turnbull, R. Feyerherm, J. J. Novoa, and M. Deumal, Dividing the spoils: Role of pyrazine ligands and perchlorate counterions in the magnetic properties of bis(pyrazine)diperchlorate copper(II), $[\text{Cu}(\text{pz})_2](\text{ClO}_4)_2$, *Inorg. Chem.* **52**, 12923 (2013).
 - [9] B. Wehinger, C. Fiolka, A. Lanza, R. Scatena, M. Kubus, A. Grockowiak, W. A. Coniglio, D. Graf, M. Skoulatos, J.-H. Chen, J. Gukelberger, N. Casati, O. Zaharko, P. Macchi, K. W. Krämer, S. Tozer, C. Mudry, B. Normand, and C. Rüegg, Giant pressure dependence and dimensionality switching in a metal-organic quantum antiferromagnet, *Phys. Rev. Lett.* **121**, 117201 (2018).
 - [10] F. M. Woodward, P. J. Gibson, G. B. Jameson, C. P. Landee, M. M. Turnbull, and R. D. Willett, Two-dimensional Heisenberg antiferromagnets: Syntheses, x-ray structures, and magnetic behavior of $[\text{Cu}(\text{pz})_2](\text{ClO}_4)_2$, $[\text{Cu}(\text{pz})_2](\text{BF}_4)_2$, and $[\text{Cu}(\text{pz})_2(\text{NO}_3)](\text{PF}_6)$, *Inorg. Chem.* **46**, 4256 (2007).
 - [11] P. Fischer, G. Frey, M. Koch, M. Könnecke, V. Pomjakushin, J. Schefer, R. Thut, N. Schlumpf, R. Bürge, U. Greuter, S. Bondt, and E. Berruyer, High-resolution powder diffractometer hrpt for thermal neutrons at sinq, *Physica B* **276**, 146 (2000).
 - [12] J. Rodríguez-Carvajal, Recent advances in magnetic structure determination by neutron powder diffraction, *Physica B* **192**, 55 (1993).
 - [13] A. M. Clogston, A. C. Gossard, V. Jaccarino, and Y. Yafet, Orbital paramagnetism and the Knight shift of d -band superconductors, *Phys. Rev. Lett.* **9**, 262 (1962).
 - [14] T. Shiroka, M. Pikulski, N. D. Zhigadlo, B. Batlogg, J. Mesot, and H.-R. Ott, Pairing of the weakly correlated electrons in the platinum-based centrosymmetric superconductor SrPt_3P , *Phys. Rev. B* **91**, 245143 (2015).
 - [15] D. L. Bryce and G. D. Sward, Solid-state NMR spectroscopy of the quadrupolar halogens: chlorine-35/37, bromine-79/81, and iodine-127, *Magn. Reson. Chem.* **44**, 409 (2006).
 - [16] F. Borsa, Phase transitions and critical phenomena in solids, in *eMagRes*, edited by R. K. Harris and R. E. Wasylshen (John Wiley & Sons, Hoboken, NJ, 2007).
 - [17] The sensitivity of the NMR relaxation rate to phase transitions arises from the so-called *critical slowing down* of fluctuations in the proximity of a transition temperature T_c . The presence of long-range spatial correlations close to T_c implies also slow time fluctuations. The latter, who match well the nuclear-spin time scales, provide a very effective relaxation channel and give rise to a peak in $1/T_1(T)$.
 - [18] A. F. McDowell, Magnetization-recovery curves for quadrupolar spins, *J. Magn. Reson. Ser. A* **113**, 242 (1995).
 - [19] V. Schettino, G. Sbrana, and R. Righini, Evidence for a phase transition in crystalline pyrazine, *Chem. Phys. Lett.* **13**, 284 (1972).
 - [20] R. K. Boyd, J. Comper, and G. Ferguson, Entropy changes and structural implications for crystalline phases of pyrazine, *Can. J. Chem.* **57**, 3056 (1979).
 - [21] P. R. Hammar, M. B. Stone, D. H. Reich, C. Broholm, P. J. Gibson, M. M. Turnbull, C. P. Landee, and M. Oshikawa, Characterization of a quasi-one-dimensional spin-1/2 magnet which is gapless and paramagnetic for $g\mu_B H \lesssim J$ and $k_B T \ll J$, *Phys. Rev. B* **59**, 1008 (1999).
 - [22] K. R. O'Neal, T. V. Brinzari, J. B. Wright, C. Ma, S. Giri, J. A. Schlueter, Q. Wang, P. Jena, Z. Liu, and J. L. Musfeldt, Pressure-induced magnetic crossover driven by hydrogen bonding in $\text{CuF}_2(\text{H}_2\text{O})_2(3\text{-chloropyridine})$, *Sci. Rep.* **4**, 6054 (2014).
 - [23] A. Le Bail, Whole powder pattern decomposition methods and applications: A retrospective, *Powder Diffr.* **20**, 316 (2005).
 - [24] M. Medarde, M. Mena, J. L. Gavilano, E. Pomjakushina, J. Sugiyama, K. Kamazawa, V. Pomjakushin, D. Sheptyakov, B. Batlogg, H.-R. Ott, M. Mansson, and F. Juranyi, 1D to 2D Na^+ ion diffusion inherently linked to structural transitions in $\text{Na}_{0.7}\text{CoO}_2$, *Phys. Rev. Lett.* **110**, 266401 (2013).
 - [25] M. Morin, E. Canevet, A. Raynaud, M. Bartkowiak, D. Sheptyakov, V. Ban, M. Kenzelmann, E. Pomjakushina, K. Conder, and M. Medarde, Tuning magnetic spirals beyond room temperature with chemical disorder, *Nat. Commun.* **7**, 13758 (2016).
 - [26] T. Shang, E. Canevet, M. Morin, D. Sheptyakov, M. Fernandez-Diaz, E. Pomjakushina, and M. Medarde, Design of magnetic spirals in layered perovskites: Extending the stability range far beyond room temperature, *Sci. Adv.* **4**, eaau6386 (2018).
 - [27] We recall that ADPs, which describe the anisotropic thermal motion through a symmetric rank-2 tensor, consist of six independent parameters. In the isotropic case, the off-diagonal terms clearly vanish. Most often U_{ij} are used to express ADPs, since they represent directly the mean-square atomic displacements (some values relevant to our case are reported in Table I). An alternative, closely related quantity is $B_{ij} = 8\pi^2 U_{ij}$. Computer programs generally output the β_{ij} values, defined as $\beta_{ij} = B_{ij} x_i^* x_j^* / 4$, since these minimize computation time and can be related directly to the reciprocal-cell parameters x_i^* and x_j^* . The diagonal ADPs describe displacements along three mutually perpendicular axes of the ellipsoid and, hence, are always positive. On the other hand, since the other elements of the ADP tensor establish the orientation of the ellipsoid with respect to the crystal-lattice coordinate system, the off-diagonal elements can be either positive or negative, under the structural constrain $\beta_{ii}\beta_{jj} > \beta_{ij}^2$, which is confirmed from our data and is a necessary requirement for the physical validity of the refinement.
 - [28] The quantities marked with (*) in Table I were constrained to be identical for the same atomic species. The occupation of the D sites was found to be very close to 100%. The occupation

of the remaining atomic sites was 100%.

[29] The Supplemental Material available at [URL] includes the two structural .cif files used for refining the neutron-

diffraction patterns at 295 K, by assuming as valid the space groups $C2$ and $C2/m$, respectively.